

The SuSAv2 Model for Inelastic Neutrino-Nucleus Scattering

J. Gonzalez-Rosa¹, **G. D. Megias**^{1,2}, **J. A. Caballero**^{1,3},
M. B. Barbaro^{4,5,6}

¹Departamento de Física atómica, molecular y nuclear, Universidad de Sevilla, 41080 Sevilla, Spain

²Research Center for Cosmic Neutrinos, Institute for Cosmic Ray Research, University of Tokyo, Kashiwa, Chiba 277-8582, Japan

³Instituto de Física Teórica y Computacional Carlos I, Granada 18071, Spain

⁴Dipartimento di Fisica, Università di Torino, 10125 Torino, Italy

⁵INFN, Sezione di Torino, 10125 Torino, Italy

⁶IPSA Paris, 94200 Ivry-sur-Seine, France

Abstract. The superscaling model SuSAv2, already available for charged-current neutrino-nucleus cross sections in the quasielastic region, is extended to the full inelastic regime. In the model the resonance production and deep inelastic reactions are described through the extension to the neutrino sector of the SuSAv2 inelastic model developed for (e,e') reactions, which combines phenomenological structure functions with a nuclear scaling function. This work also compares two different descriptions of the Δ resonance region, one based on a global scaling function for the full inelastic spectrum and the other on a semi-phenomenological Δ scaling function extracted from (e,e') data for this specific region and updated with respect to previous work. The results of the model are tested against (e,e') data on ^{12}C , ^{16}O , ^{40}Ca and ^{40}Ar and applied to the study of the charged current inclusive neutrino cross-section on ^{12}C and ^{40}Ar measured by the T2K, MicroBooNE, ArgoNEUT and MINERvA experiments, thus covering several kinematical regions.

1 Introduction

Current long-baseline neutrino experiments explore various fundamental questions, like leptonic CP violation, neutrino oscillations and mass hierarchy. In these experiments, which operate at energies from hundreds of MeV up to tens of GeV, there are numerous mechanisms that contribute to the nuclear response, such as quasielastic processes, multi-nucleon excitations and different contributions from the inelastic regime. Accordingly, theoretical analyses have been developed to describe these contributions by using detailed nuclear models. The quasi-elastic regime can be reproduced by models like SuSAv2 [5]. Other channels like two-particle two-hole or the Δ resonance region have been studied within the same model [1–4]. However, there is still a lack of knowledge regard-

ing higher resonance (HR) and the deep inelastic scattering (DIS) regimes [6]. In this study, neutrino interaction models for the inelastic regime are explored.

Inclusive charged-current (CC) neutrino-nucleus scattering cross sections have been measured in various experiments and at different energy regimes. In the T2K [12], MicroBooNE [19] or SciBooNE [14] experiments, the main contributions to the cross sections are quasielastic (QE), one pion (1π) production and two-particle two-hole (2p2h) meson-exchange current (MEC), being QE the dominant one [12]. Nevertheless, other experiments such as MINERvA [18], NOvA [15], ArgoNEUT [16] or the forthcoming DUNE [13] operate at higher kinematics, in which the inelasticities, like HR or DIS, become more important [16]. Here we focus in the T2K [12], MINERvA [18], MicroBooNE [19] and ArgoNEUT [16] measurements.

In this work, we update and extend two models based on the SuperScaling Approach (SuSA) [7], the Relativistic Mean Field (RMF) [8] ingredients included in the SuSAv2 model and an analysis of inclusive (e, e') data. First, we focus on the Δ resonance region and update our previous semi-phenomenological model for this region, which it is labeled as "SuSAv2- Δ ". Second, we present an extension of the SuSAv2-inelastic for electrons [3] to the neutrino sector referred as "SuSAv2-inelastic".

2 Methodology

We use the so-called SuSAv2 model [5] which improves the original prescription (SuSA) by means of the RMF theory. This allows to build a more sophisticated theory-based approach that reproduces very well the superscaling behavior shown by electron scattering data while improving the description of the transverse channel. This model, which was originally developed for the QE regime, was extended to the Δ resonance region and to the full inelastic regime [3]. This second case was only available for electrons. Here we extend it for the first time to neutrinos [4].

In the SuSAv2- Δ model, we obtain a semi-phenomenological Δ scaling function to be used in the Δ resonance region. The latest version of SuSAv2-MEC (SuSAv2-QE and 2p2h model) is used to remove QE and 2p2h contributions from the data [1]. In a similar way, contributions beyond Δ resonance (HR + DIS) are removed by applying the SuSAv2-inelastic model. By this method we isolate Δ -resonance contributions from inclusive electron scattering experimental cross section:

$$\left(\frac{d^2\sigma}{d\Omega_e d\omega}\right)^\Delta = \left(\frac{d^2\sigma}{d\Omega_e d\omega}\right)^{\text{exp. data}} - \left(\frac{d^2\sigma}{d\Omega_e d\omega}\right)^{\text{SuSAv2-QE}} - \left(\frac{d^2\sigma}{d\Omega_e d\omega}\right)^{2p2h} - \left(\frac{d^2\sigma}{d\Omega_e d\omega}\right)^{\text{HR + DIS}}. \quad (1)$$

Then, dividing the result by the elementary $N \rightarrow \Delta$ cross section

$$f^\Delta(\psi_\Delta) = k_F \frac{\left(\frac{d^2\sigma}{d\Omega_e d\omega} \right)^\Delta}{\sigma_{\text{Mott}}(v_L G_L^\Delta + v_T G_T^\Delta)}, \quad (2)$$

we obtain a semi-phenomenological scaling function for the Δ regime.

As commented before, the SuSAv2-inelastic model, which is an extension of the SuSAv2-QE formalism to the complete inelastic spectrum - resonant, non-resonant and deep inelastic scattering-, originally developed for electron reactions [3] is here extended to the neutrino sector. The inelastic nuclear responses are obtained by integrating the nuclear responses depending on the final-state reduced invariant mass (μ_X) over all possible final hadronic states [5],

$$R_K^{\text{inel}}(\kappa, \tau) = \frac{Nm_N^3}{k_F^3 \kappa} \xi_F \int_{\mu_X^{\text{min}}}^{\mu_X^{\text{max}}} d\mu_X \mu_X f^{\text{model}}(\psi_X) G_K^{\text{inel}}. \quad (3)$$

The limits for the complete inelastic spectrum are

$$\mu_X^{\text{min}} = 1 + \frac{m_\pi}{M_N}; \quad \mu_X^{\text{max}} = 1 + 2\lambda - \frac{E_s}{M_N}. \quad (4)$$

The lower limit μ_X^{min} can be varied depending on whether the Δ region is included or excluded. The factor G_K^{inel} includes two inelastic structure functions (F_1 and F_2) for electrons and three (F_1 , F_2 and F_3) for neutrinos.

In Figure 1, we show the inelastic structure function with the different parametrizations: Bodek-Ritchie (BR) [9], Bosted-Christy (BC) [10] and parton distribution functions (PDF) [11]. Both BR and BC reproduce the shape of the resonances, while PDF shows an average of these resonances. At higher Q^2 -values, the three parametrizations match.

In the region of moderate and large x -values, the neutrino inelastic structure functions can be related to the electromagnetic ones through [6]:

$$F_{1,2}^{\nu N} \approx \frac{18}{5} F_{1,2}^{eN}. \quad (5)$$

The additional structure function in weak interactions, i.e. F_3 , can be written using the quark distributions [6],

$$xF_3^{\nu N} = x(d(x) + u(x) + s(x) + \bar{s}(x) - \bar{u}(x) - \bar{d}(x) - c(x) - \bar{c}(x)), \quad (6)$$

where $u(\bar{u})$, $d(\bar{d})$, $c(\bar{c})$ and $s(\bar{s})$ are the distributions for the up, down, charm and strange quarks (antiquarks), respectively. These approximations based on QCD theory are valid at high kinematics ($Q^2 > 3.0 \text{ GeV}^2$). Additionally, the proposal given by the Bodek-Ritchie parametrization [9] connects F_3 and F_2 by

$$xF_3^{\nu N} = F_2^{\nu N} - 2\bar{Q}(x), \quad (7)$$

The SuSv2 Model for Inelastic Neutrino-Nucleus Scattering

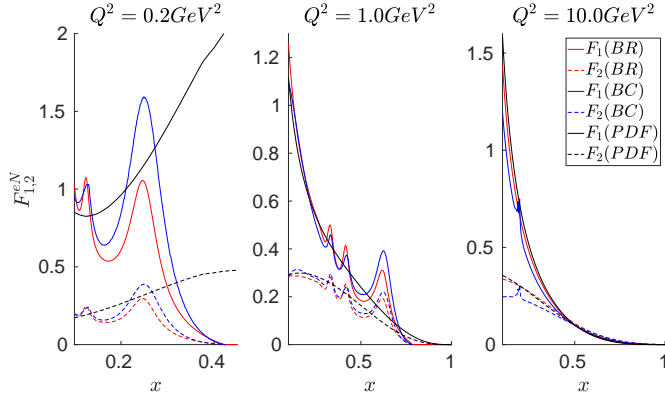


Figure 1. Electromagnetic inelastic structure function ($F_{1,2}$) displayed as a function of the Bjorken variable [9] at three different kinematics $Q^2 = 0.2$ (left), 1.0 (center) and 10 (right) GeV^2 for three different parametrizations: Bodek-Ritchie [9], Bosted-Christy [10] and PDF [11].

where the antiquark distribution, $\bar{Q}(x)$, is defined in terms of empirical fits of electron scattering data under some approximations. Both options are explored in our work [4].

In Figure 2, we show the F_3 inelastic structure function and antiquark distribution for different kinematics and parametrizations. BR and PDF antiquarks distributions are different but they share the same order of magnitude. The differences between the parametrizations are similar to the ones shown in Figure 1.

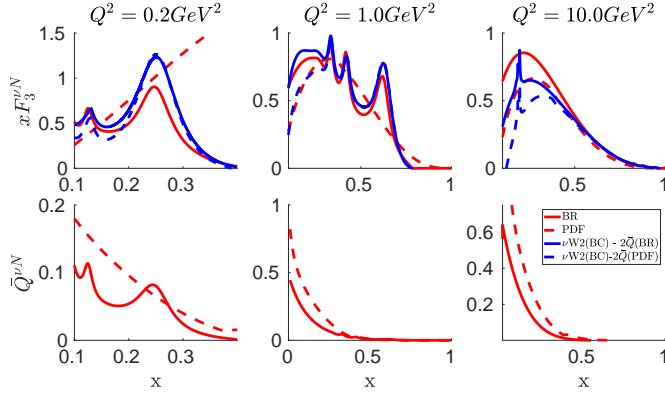


Figure 2. Neutrino inelastic structure function ($x F_3$) and antiquark distribution (\bar{Q}) displayed as a function of the Bjorken variable. The kinematics and parametrizations are the same as in Figure 1

3 Results

3.1 Electron scattering

As a first step, we test our model for electron scattering. In Figure 3, we show the double differential inclusive cross section for electron-nucleus (^{12}C) scattering. In order to explain the experimental data it is necessary to consider all reaction channels, i. e., QE, 2p2h and inelastic contributions. The inelastic contributions are obtained using two methods: the SuSAv2-inelastic for the whole inelastic spectrum (Full inelastic) or the SuSAv2- Δ working alongside SuSAv2-inelastic for higher resonances and deep inelastic scattering (Δ + DIS), being the latter more appropriate for neutrinos due to the limitations of the structure functions defined in Section 2. Furthermore, we also consider different parametrizations for the inelastic structure functions: Bodek-Ritchie (BR) [9], Bosted-Christy (BC) [10] or Parton Distribution Function (PDF) [11]. As we see, the Full inelastic model tends to reproduce well the data [3] although, there is some overestimation of the data for 37 and 45. In general, the Δ + DIS model gives results similar to the full inelastic model but it tends to underestimate the experimental data at higher values of the scattering angle.

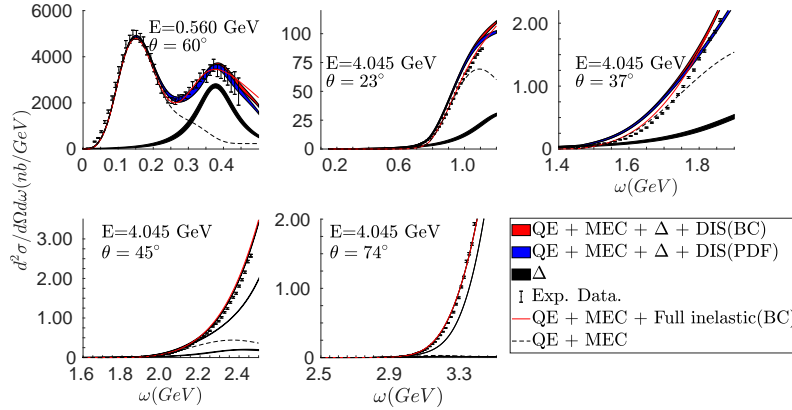


Figure 3. Double-differential inclusive cross section for $e^{-12}C$ scattering at given beam energies and scattering angles (labeled in the panels). It is displayed as a function of the transferred energy. Data from [17].

We extend our studies to other nuclei ($^{16}O, ^{40}Ar, ^{40}Ca$). In Figure 4, the experimental data are successfully described by the models and both parametrizations overlap. However, there are discrepancies, specially around the delta peak. In general, Δ + DIS model provides good agreement with data which gives us confidence in using this model for neutrino scattering.

The SuSAv2 Model for Inelastic Neutrino-Nucleus Scattering

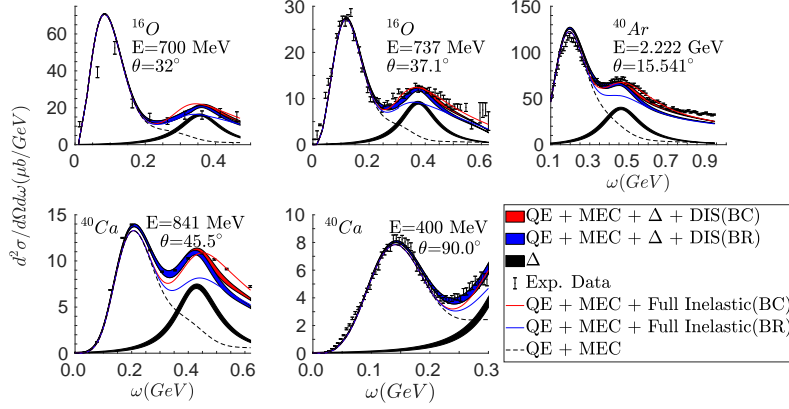


Figure 4. Same as fig. 3, except now for oxygen (top left panels), argon (top right) and calcium (bottom) and different kinematics. Data from [17].

3.2 Neutrino scattering

In this section, we test our predictions against the data from T2K, Minerva, MicroBooNE and ArgoNEUT experiments.

For T2K, the flux peaks at 0.6 GeV and the target is carbon. In Figure 5, we show the double-differential inclusive cross section. The three parametrizations give us similar results, but in general for T2K, the QE contribution is dominant in all cases although inelastic contributions are also relevant at forward angles. For muon momentum over 1.5 GeV, the contribution of DIS is more important and it is essential to explain the data. At very forward angles, the models tend to overestimate the data in the region of the QE peak. This can be addressed using the relativistic mean field model which introduces a more accurate description of nuclear dynamics and final-state interactions at low kinematics. Nevertheless, the data are reproduced nicely in general.

In the case of Minerva, the energy flux peaks at 3.5 GeV and the target is hydrocarbon. In Figure 6, we represent the single-differential cross section in function of the longitudinal (p_L) and transverse (p_T) momentum. The contribution of QE and 2p2h channels are around 50% of the cross section. These results are in accordance with the MnvGenie model used in the MINERvA MonteCarlo generator [18]. The addition of the DIS contribution shifts the maximum to the right for transverse momentum and the opposite for longitudinal. Regarding the comparison to data, we underestimate the data around 20%. Further studies are needed to establish the validity of the model and the applicability regime.

For MicroBooNE, the energy flux peaks at 0.8 GeV and the target is argon. The results shown in Figure 7 are similar to those in T2K, showing also a reasonable agreement with data. However, at backward angles the prediction is shifted

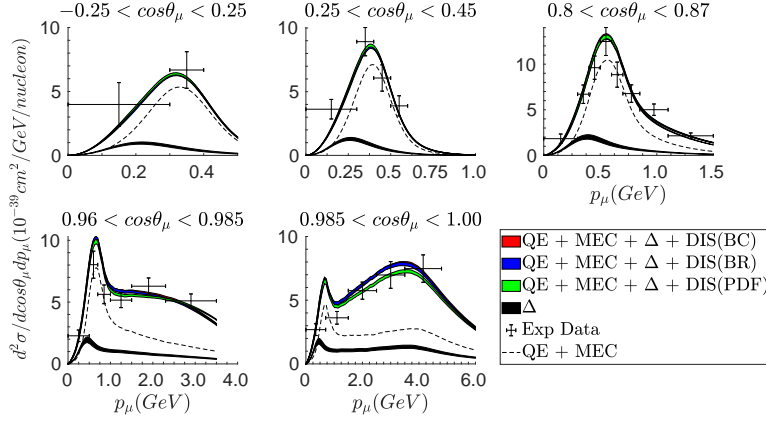


Figure 5. The CC-inclusive T2K flux-folded ν_μ - ^{12}C double differential cross section per nucleon, for different bins in the muon scattering angle -labeled in the panels. It is displayed as a function of the muon momentum. The data come from [12].

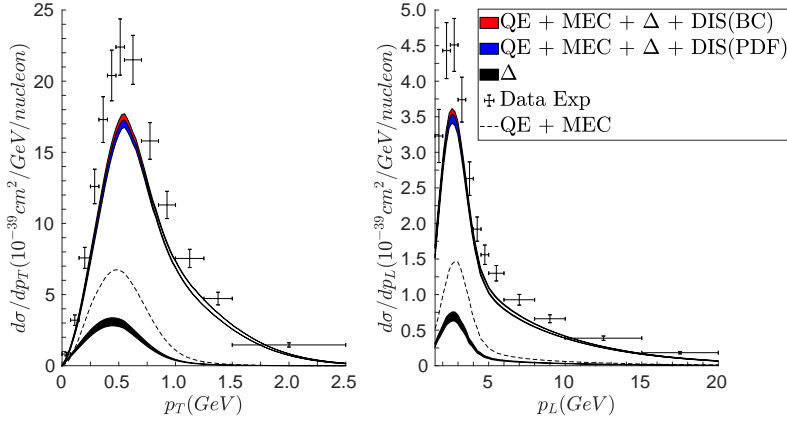


Figure 6. The CC-inclusive Minerva flux-folded ν_μ - ^{12}C single differential cross section per nucleon as a function of the muon longitudinal (right) and transverse (left) momentum. Data from [18].

to lower values of muon momentum, and the reverse occurs at forward angles. This is consistent with the experimental MonteCarlo analyses [19].

For ArgoNEUT, the target is argon and the neutrino and antineutrino energy flux peaks at 9.6 and 3.6 GeV, respectively. In Figure 8, we show the single differential cross section using Bodek-Ritchie and PDF parametrizations. Contrary to the other cases, there are significant differences between these two approaches for neutrinos. This could be connected to the larger energy in ArgoNEUT for

The SuSAv2 Model for Inelastic Neutrino-Nucleus Scattering

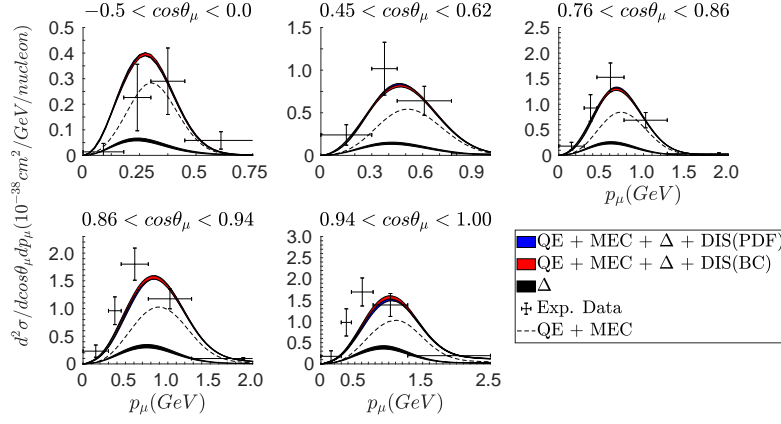


Figure 7. The CC-inclusive MicroBooNE flux-folded ν_μ - ^{40}Ar double differential cross section per nucleon in bins of the muon scattering angle as a function of the muon momentum. Data taken from [19].

neutrinos as they are rather similar for antineutrinos. Similar to the Minerva case, we underestimate the data for neutrinos in ArgoNEUT. On the contrary, the antineutrino cross section is very well reproduced.

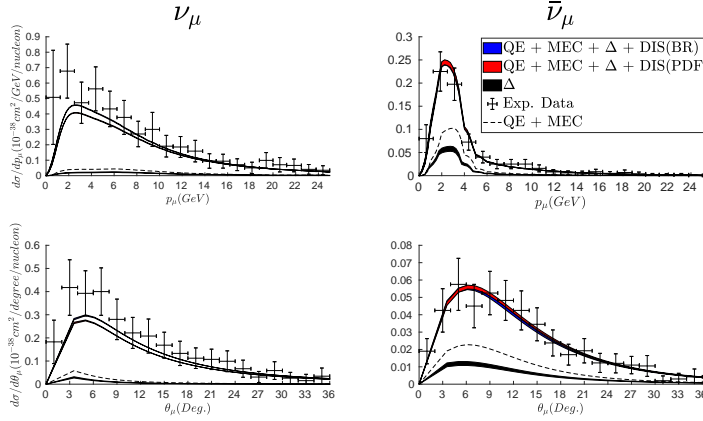


Figure 8. The CC-inclusive ArgoNEUT flux-integrated $\nu_\mu(\bar{\nu}_\mu)$ - ^{40}Ar single differential cross section per nucleon, displayed as a function of the muon momentum (top) or the muon scattering angle (bottom). The data come from [16].

4 Conclusion

The SuperScaling model has been tested against electron-nucleus reactions for different nuclear regimes, reproducing cross section data throughout the energy spectrum. A new model for the Δ resonance region (SuSAv2- Δ) has been developed for both electron and neutrino interactions together with an extension of the SuSAv2-inelastic model to the neutrino sector. Weak inelastic structure functions were obtained by using relationships among the electromagnetic inelastic structure functions given by QCD. This description fails at intermediate-high energies. Therefore, the SuSAv2- Δ approach is applied at these kinematics. Our predictions have been compared with available data for charged current muon neutrino-nucleus reactions from the T2K, MINERvA, MicroBooNE, and ArgoNEUT experiments. For T2K, the QE channel dominates in most of the kinematical situations. At forward angles, the contribution of DIS gets larger and becomes crucial to explain the experiment. Similar comments also apply to MicroBooNE. The discrepancies between the data and theoretical predictions are consistent with the studies based on Monte Carlo analyses and other theoretical calculations. For MINERvA and ArgoNEUT, the DIS contribution dominates in most kinematics explored. An interesting outcome of this study is that in the case of neutrinos, for both MINERvA and ArgoNEUT, the predictions are below the data in the region where the cross sections reach their maxima, whereas the description of ArgoNEUT data for antineutrinos is excellent. This can be connected with the different kinematics explored and calls for an improved description of the high energy region.

The present study shows clearly the applicability of the SuSAv2 model to describe weak processes. This can be seen in more detail in [4]. Although further studies are needed with new ingredients implemented, like the dynamical coupled channels model (DCC) [20], we believe that this work can provide helpful information for the analyses of present and future experiments on neutrino oscillations.

Acknowledgments

This work was partially supported by the Spanish Ministerio de Ciencia, Innovación y Universidades and ERDF (European Regional Development Fund) under contract PID2020-114687GB-100, by the Junta de Andalucía (grants No. FQM160, SOMM17/6105/UGR and P20-01247), by University of Tokyo ICRR's Inter-University Research Program FY2020 and FY2021, by the INFN under project Iniziativa Specifica NucSys and the University of Turin under Project BARM-RILO-20 (M.B.B.), by the EU's H2020 research and innovation programme under the Marie Skłodowska-Curie grant agreement No. 839481 (G.D.M.). J.G.R. was supported by a Contract PIF-PPITUS 2020) from the University of Seville (Plan Propio de Investigación y Transferencia) associated with the project PID2020-114687GB-100.

References

- [1] M.V. Ivanov et al., *J. Phys. G: Nucl. Part. Phys.* **43** (2016) 045101.
- [2] J.E. Amaro et al., *Phys. Lett. B* **696** (2011) 151155.
- [3] G.D. Megias et al., *Phys. Rev. D* **94** (2016) 013012.
- [4] J. Gonzalez-Rosa et al. *Phys. Rev. D* **105** (2022) 093009.
- [5] G.D. Megias, Charged-current neutrino interactions with nucleons and nuclei at intermediate energies. PhD thesis, University of Seville (2017).
- [6] M. Sajjad Athar and J.G. Morfín, *J. Phys. G: Nucl. Part. Phys.* **48** (2021) 034001.
- [7] J.E. Amaro et al., *Eur. Phys. J. Special Topics* **230** (2021) 4321.
- [8] R. Gonzalez-Jimenez et al., *Phys. Rev. D* **97** (2018) 013004.
- [9] A. Bodek and J.L. Ritchie, *Phys. Rev. D* **23** (1981) 1070.
- [10] M.E. Christy and P.E. Bosted, *Phys. Rev. C* **81** (2010) 055213.
- [11] M. Glück et al., *Eur. Phys. J. C* **5** (1998) 461.
- [12] K. Abe et al. (T2K Collaboration), *Phys. Rev. D* **98** (2018) 012004.
- [13] R. Acciarri et al. (DUNE Collaboration), arXiv:1512.06148.
- [14] Y. Nakajima et al. (SciBooNE Collaboration), *Phys. Rev. D* **83**, 012005 (2011).
- [15] M. A. Acero et al. (NOvA Collaboration), *Phys. Rev. Lett.* **123**, 151803 (2019).
- [16] R. Acciarri et al. (ArgoNEUT Collaboration), *Phys. Rev. D* **89**, 112003 (2014).
- [17] O. Benhar, D. Day, and I. Sick, arXiv:nucl-ex/0603032 (2006)2.
- [18] A. Filkins et al. (MINERvA Collaboration), *Phys. Rev. D* **101**, 112007 (2020).
- [19] P. Abratenko et al. (MicroBooNE Collaboration), *Phys. Rev. Lett.* **123**, 131801 (2019).
- [20] S.X. Nakamura et al., *Phys. Rev. D* **92** (2015) 074024.